ACS APPLIED MATERIALS & INTERFACES

Research Article

www.acsami.org

Interfacial Adhesive Properties between a Rigid-Rod Pyromellitimide Molecular Layer and a Covalent Semiconductor via Atomistic Simulations

Maxim A. Makeev,[†] Philippe H. Geubelle,[‡] Nancy R. Sottos,[§] and John Kieffer*,[†]

[†]Department of Materials Science and Engineering, University of Michigan, Ann Arbor, Michigan 48109, United States

[‡]Department of Aerospace Engineering, University of Illinois at Urbana−Champaign, Urbana, Illinois 61801, United States

[§]Department of Materials Science and Engineering, University of Illinois at Urbana−Champaign, Urbana 61801, Illinois, United States

ABSTRACT: We conducted a comprehensive atomistic simulation study of the adhesive properties of aromatic rigid-rod *poly-[(4,4′diphenylene) pyromellitimide]* on a dimer-reconstructed silicon surface. We describe the structural developments within the adherent's interfacial region at the atomistic scale, and evaluate the energetics of the adhesive interactions between bimaterial constituents. In particular, we observe a transition between noncontact and contact adhesion regimes as a function of the interfacial bonding strength between the polyimide repeat units and the silicon substrate. This transition is manifest by a three- to four-fold increase in adhesive energy, which is entirely attributable to structural relaxation in the organic layer near the interface, revealing the importance of accurately describing structural details at interfaces for reliable interfacial strength predictions. The underlying molecular reconfigurations in the pyromellitimide layer include preferred orientation of the rigid-rod molecules, molecular stacking, ordering, and the local densification. The role of each of these factors in the adhesive behavior is analyzed and conclusively described. Where possible, simulation results are compared with theoretical model predictions or experimental data.

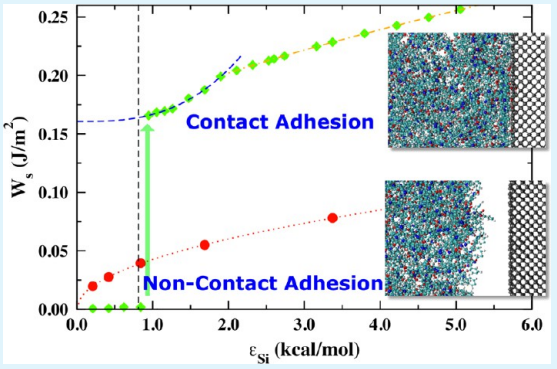

KEYWORDS: *adhesion, interface, polyimide, molecular dynamics, glass transition, structure−property relations*

1. INTRODUCTION

Thin polymeric coatings (with thickness ranging from a few hundred nanometers to several micrometers) have become indispensable and integral parts of microelectronic devices and other technological applications.[1,2] In this context, particular attention has been paid to rigid or semirigid aromatic polyimide polymers,[3,4] which are now widely employed as passivation (anticorrosion shell) layers, dielectric insulators, alignment layers for liquid crystal displays, gas separation films, structural layers in the microelectromechanical and semiconductor electronic devices, and protective coatings (e.g., matrix resins for fiber reinforced plastics).[4] Such a remarkably broad spectrum of application areas is derived from superior thermo-mechanical properties of polyimide-based materials, including low surface roughness and heat resistance. For a number of technological applications, the superb thermal stability of polyimides (in excess of 450 °C, for some) is of great essence. This property stems from a specific hybridization of orbitals in the aromatic rings of polyimide molecules. Also noteworthy is the fact that the coefficient of thermal expansion of polyimide layers matches that of semiconductors well, which is a great asset to complement the low dielectric coefficient and the remarkable mechanical properties of polyimide films.[3] All the aforementioned areas of applications, however, require integration of polyimide layers into complex device architectures so that the packaging process does not interfere with the device performance or operation. The key issue, intimately related to such integration processes, is adhesion.[5] It has long been realized that both thermal and mechanical properties of interfaces are largely defined by adhesion. Consequently, detailed and in-depth understanding of adhesive behavior of polyimide layers on covalent semiconductors at the molecular level has become a necessity.

Further progress in the device packaging and coating technology requires a deeper understanding of the processes that control structural developments within the interfacial layer of polyimide deposited on chemically dissimilar substrates, that is, inorganic materials. To date, nearly all theoretical studies of adhesion-related phenomena for organic matter deposited on covalent semiconductors, have focused either on single-molecule physi- or chemisorption, treated using advanced quantum chemistry methods[6−10] or development of various continuum elasticity/mechanics-based approaches to the problem of adhesion.[11−15] While the former approaches

Received: December 14, 2012
Accepted: April 22, 2013
Published: April 22, 2013

   dx.doi.org/10.1021/am3031163 | ACS Appl. Mater. Interfaces 2013, 5, 4702−4711

provide detailed and precise information about the corresponding systems, they lack the desired level of robustness and predictive capabilities for realistic-size systems. This is, largely, because of (1) limitations in system size (few hundreds atoms, at best) and because (2), until recently, quantum mechanical approaches have not included van der Waals (vdW) interactions, even though these appear to dominate interface energetics of bimaterials comprised of a soft organic polymer and a covalent solid. Another main thrust in the quantum calculation-based studies of adhesion has been on understanding the mechanism of cohesion in crystalline solids and adhesion in dissimilar crystalline bimaterials.[16−19] For metallic and ceramic systems, it was found that the cohesive (adhesive) energy scales with the average de Broglie lengths of the paired constituents, thus leading to a semiquantitative description of adhesive energy in bimaterial systems.[16] However, the existing theoretical framework is not suitable for materials with significant vdW contributions. On the other hand, the continuum-level treatments[10−15] do not adequately incorporate all microscopic details of the interfaces, that is, they treat interfaces in an oversimplified manner, especially concerning the relationship between interface microstructure and energetics. All of the above suggests that there is a need to further our understanding of adhesive behavior via the development of theoretical and simulation-based models, specifically concerning bimaterial systems in which soft organic and covalently bonded inorganic constituents are paired.

In the present study, we focus on the most fundamental aspects of the adhesion phenomenon, scrutinized via classical atomistic simulations. A few studies, laying out the grounds for elaborate classical simulation treatments of the polymer adherent layers deposited on solid substrates have previously been reported.[20−22] However, these studies focused on different issues than we report here. By employing large-scale classical molecular dynamics (MD) simulations, we aim to elucidate, in as much detail as possible, the effects of the interfacial structure on the adhesive behavior between polyimide layers of a few nanometers thickness and bulk silicon. Although the true nature of adhesive-adherent interaction is still poorly understood, there are strong indications that vdW forces play a predominant role in the adhesion-related phenomena.[23] Consequently, we focus our attention to the dispersive coupling between adhesive and substrate. In particular, by varying the potential well depth of the 6−12 Lennard-Jones interactions across the interface, we reveal a transition between noncontact and contact adhesion in quenched polyimide layers as a function of the interaction strength across the interface. In the regime of strong interface coupling, the dependences of the adhesive energy on the vdW interaction strength as well as on the structural features of the interface are identified and discussed in detail.

2. COMPUTATIONAL DETAILS

2.1. Model Polyimide. The model polyimide, we investigated in this study, consists of aromatic rigid-rod poly-[(4,4′diphenylene) pyromellitimide] (PMB) repeat units. The structure of its crystal unit cell has been previously reported.[24,25] The molecular structure of PMB monomer (created from the data Table 1 of ref 25 based on X-ray diffraction data) is depicted in Figure 1. As made explicit in ref 25, PMB may exist in two conformational configurations, the principal difference between the two being the value of dihedral angle of the biphenyl moiety. In the present work, we employed the model, where this angle is $\theta_1 = 0.4°$. Under this assumption, the conformational

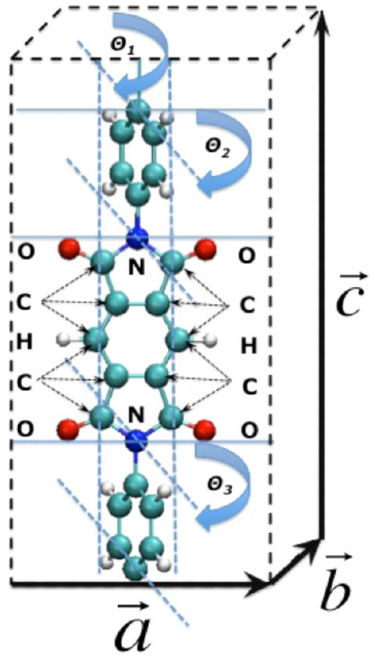

Figure 1. Sketch of an elementary unit of the PMB. The lattice parameters of the unit cell are |a| = 8.57 Å, |b| = 5.51 Å, and |c| (fiber-axis) = 16.78 Å. The dihedral angle between phenyl rings, $\theta_1 = 0.0°$. Each biphenyl moiety is rotated with respect to the fiber axis by $|\theta_2| = |\theta_3| = 65.0°$, so that the following equality holds: $\theta_1 + \theta_2 + \theta_3 = 0$.

angles are $\theta_2 = -65.0°$ and $\theta_3 = 65.0°$ (see Figure 1 for illustration and notations used).

2.2. Classical Interaction Potential Scheme. All classical (MD) simulations,[26] reported herein, were performed using the DLPOLY classical MD simulation package.[27−29] In our simulations, we largely employed a modified AMBER force field[30] to describe bond-stretching, bond-bending, dihedral angular (including the improper, out-of-plane contributions) interactions, and vdW coupling between PMB molecules. Accordingly, the total potential energy of a multimolecule PMB system consists of the following contributions:

$$E = E_r + E_\theta + E_\phi + E_{im} + E_{vdW} + E_q \quad (1)$$

where E_r corresponds to bond-stretching, E_θ to bond-bending, E_ϕ to the dihedral contribution, E_{im} to improper dihedral, E_{vdW} to the van der Waals pair interactions, and E_q to the Coulombic interactions between partial charges. In our study, all the Coulombic interactions have been treated using the Ewald summation method, as implemented in the DLPOLY package.[31] A number of extensions were introduced to the aforedescribed scheme to rectify the energetics of C−N and C−O bonds by using corresponding parameters from ref 32. Additionally, to account for dielectric nature of the polyimide medium, the characteristic value of $\epsilon_d \approx 3.4$ for the dielectric constant of polyimides was used in the long-range interaction scheme. The partial charges on PMB atoms were computed using Gaussian ab initio package.[33] Specifically, to compute the partial charges on PMB atoms, we employed the Merz−Singh−Kollman method, as implemented in the Gaussian 09 package.[34,35] The computed partial charge sets are summarized in Figure 2 (lower panel). In our simulations, we employed the set of partial charges obtained using B3LYP pseudopotentials with 6-31G(d,p) basis sets. Furthermore, we investigated in detail as to how the results are affected by the charge variations (in the range defined by data sets shown in Figure 2) and found that the effect of partial charge localization on dispersive interactions does not introduce substantial corrections or change conclusions contained herein.

2.3. Preparation and Characterization of Amorphous Systems. All initial atomic configurations of amorphous PMB repeat units have been generated using the rotational isomeric state (RIS)

dx.doi.org/10.1021/am3031163 | ACS Appl. Mater. Interfaces 2013, 5, 4702−4711

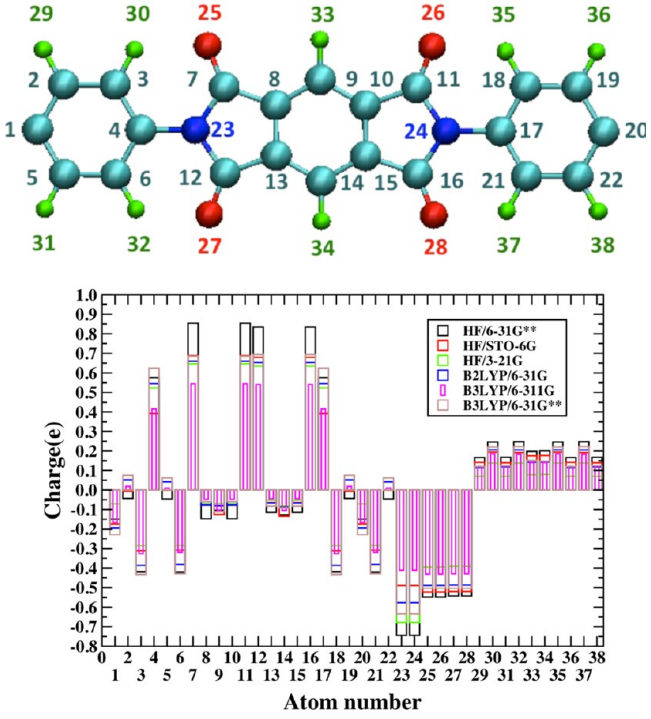

Figure 2. Upper panel: Atomic structure of a single PMB unit, with atoms of the unit cell marked by numbers. Lower panel: Partial charges on PMB atoms computed via five different basis sets or pseudopotentials, as detailed in the figure legend.

method, as originally developed and described by Theodorou and Sutter,[36] which has been extensively employed for building atomically resolved and coarse-grained amorphous polymer configurations. The initial density of the thus prepared systems was fixed at ∼1.2 g/cm^3. Thereby, molecular configurations with a total of 634 molecules (each consisting of 38 atoms, as shown in Figure 1) were built. The bond between the phenylene rings provides a flexible connection between the rigid polyimide repeat units. Here, we report results for a system in which these bonds are not yet formed, which allows for the highest degree of structural relaxation on MD time scales while preserving the geometric constraints associated with the principal polymer building block. The present findings therefore serve as a benchmark for gauging the effects on adhesive properties that can be attributed to proper structural relaxation near the interface, and thus, justifying the need for following realistic assembly protocols in polymerized systems. Each amorphous configuration has been equilibrated for over 250 ps, at T = 900 K and ambient pressure, the MD time step being τ_{MD} = 0.1 fs. In the course of relaxation, periodic boundary conditions (PBC) were applied in all three directions to the varied-volume, parallelepiped shape MD simulation cell. For the simulations reported here we used either NVT or NPT conditions, with the Berendsen thermo- or barostat[37] applied to the system whenever appropriate. For the temperature and pressure control, the pressure relaxation time was fixed at τ_P = 0.5 ps and temperature relaxation time was τ_T = 0.1 ps. Such prolonged and fine-time-step relaxations allow one to reach true minimum-energy amorphous PMB states (under constraints imposed by the potential scheme employed in this work). Subsequently, one of the prepared samples, fully equilibrated at T = 900 K, has been quenched into a disordered (glassy) phase in steps of temperature ΔT = 25 K, with prolonged relaxation (∼200 ps) between the quenching steps. Thereby, a set of equilibrated atomic configurations of amorphous PMB was obtained, in the temperature range between T = 5 and 900 K, with density, specific volume, and radial distribution functions, computed for each of these equilibrium states.

Structural characterization of the amorphous phase of the polyimide sample equilibrated at room temperature is based on pair correlation function (PCF) analysis. Shown in Figure 3 are the PCFs of the liquid

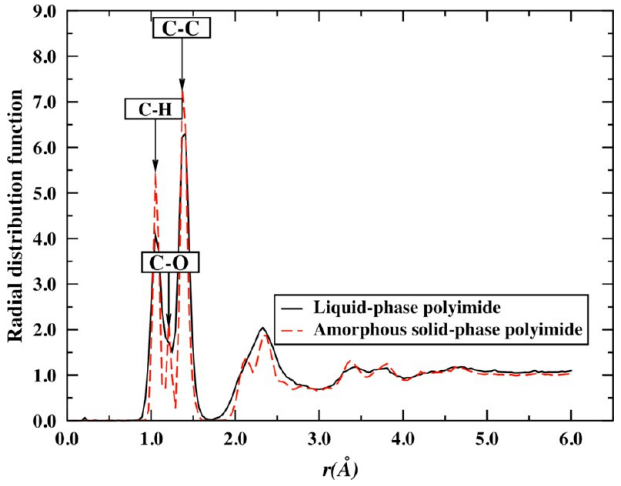

Figure 3. Radial distribution functions for the liquid-phase (solid line) and amorphous (dashed line) solid-phase PMB samples. The average interatomic distances of atoms pertaining to a single polyimide molecule are marked on the figure.

and amorphous phases of polyimide sample. As can be observed in this figure, the solid-phase polyimide possesses all the features of an amorphous configuration. The heights and widths of the first and second peaks follow the conventional trends, characteristic for the transition from a liquid to a glassy state upon quenching. First, the apparent sharpening of the peaks occurs in the solid-phase. Second, we also observe the characteristic second peak splitting, which arises because of a specific relative positioning of atoms or molecules in an amorphous phase. In brief, the effect is due to a particular distribution of intermolecular distances and not intrinsic to the configuration of atoms within individual molecules.[38] The first peak shows subpeaks revealing C−H (1.04 Å), C−O (1.20 Å), and C−C (1.37 Å) interatomic distances, as indicated in the figure. No long-range order in the amorphous state is observed; this behavior is essentially the same as in the liquid phase. We therefore conclude that the quenched and equilibrated sample represents a realistic model of an amorphous polymer.

The glass transition temperature, T_g, was computed based on the crossing between the linear fits to the temperature dependent density above and below the glass transition.[39] The simulation data were obtained at a fixed cooling rate of 10 K/ps. An illustration of the vitreous PMB configuration and the temperature dependence of the specific volume are shown in Figure 4. The value of $T_g \approx 708$ K so obtained falls well within the range between 705 and 715 K, experimentally determined glass transition temperatures of PMB systems, using two different methods.[40] The slope of the density versus temperature, which is linear in the region of the solid-phase PMB (see Figure 4b), gives the coefficient of thermal expansion (CTE) at a given pressure and temperature via

$$\beta = -\frac{1}{3\rho}\left(\frac{\partial \rho}{\partial T}\right)_P \qquad (2)$$

where $\rho = \rho(T)$ is the temperature dependent density of model polyimide and P is the pressure, which was kept constant (ambient) in our simulations. From the simulation data, we compute the room temperature (T = 300 K) CTE as $\beta_{PI}^{T} = 64.98 \times 10^{-6}$ K^{-1}. This value fits rather well in the range of experimental CTE values for polyimide polymers: $\beta_{PI}^{E} \approx 8.0-65.0 \times 10^{-6}$ K^{-1}.[41]

2.4. Si(001) Substrate. The covalently bonded solid substrate, employed in this work, was that of model Si(001). The well-known Tersoff empirical bond-order interatomic potential was employed to describe the interactions between silicon atoms.[42] The model silicon surface was (2 × 1) dimer-reconstructed. This surface configuration has been reported to be the most stable in numerous studies. The total number of silicon substrate atoms was N_{Si} = 18,720 throughout the

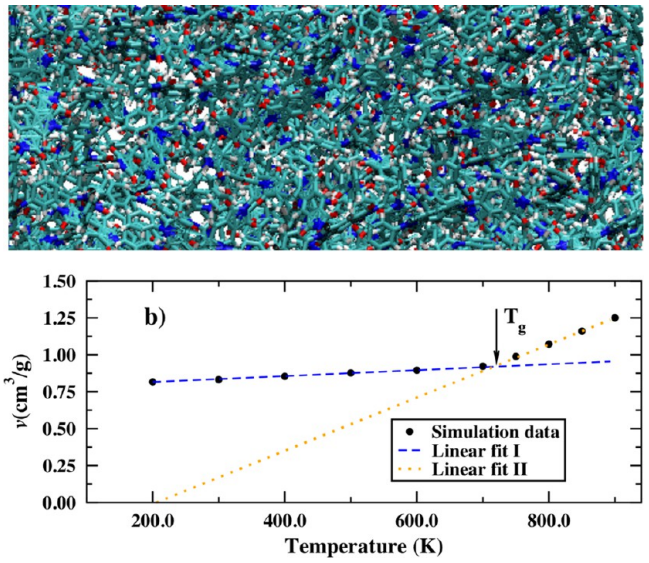

Figure 4. (a) Snapshot of one-half of the glassy PMB configuration, taken at T = 300 K (bond representation). (b) Temperature dependence of the specific volume obtained via rapid quenching of the PMB sample is shown for the pure PI atomic configuration consisting of 634 molecules. The solid and liquid regimes are identified by different slopes of the linear dependences. The point of transition to the amorphous state is marked by an arrow.

simulations. The lateral and vertical extents of the Si(001) slab were fixed at 65.17 Å × 65.17 Å × 70.00 Å. The initial configuration was relaxed for τ_R = 100 ps (MD time step being τ_{MD} = 1.0 fs), at ambient conditions. This allowed for a nearly complete relaxation of all built-in stresses, including those at the dimer-reconstructed surface, while keeping the surface reconstruction intact.

It is well-known that a surface of a covalent solid can bear significant amount of charge (under condition of electroneutrality). This might contribute significantly to the chemisorption and physisorption phenomena, both in terms of the interface energetics and chemical reactions between substrate and sorbent.[43] For example, it is known that the dielectric constant is strongly affected by the nature of the bonding between substrate and adsorbent. In a first approximation, however, for the present study, we neglect possible effects that a charged silicon surface and the force damping due to the dielectric screening may have on adhesion interactions. This simplification is justified as the inclusion of these complex refinements would only add a constant and comparably minor bias to adhesion energies and forces examined during our parametric analysis. Moreover, the effect of dipolar interactions that arise from surface charges are implicitly contained in the vdW interactions, which we systematically vary.

2.5. Si(001)−Pyromellitimide Bimaterial and Interface. The model bimaterial system under consideration, which consists of PMB repeat units adhering to a silicon substrate, was prepared as follows. A series of PMB amorphous configurations were generated by stepwise quenching molten PMB into the glassy state. From this series we chose the room temperature configuration and further relaxed it isothermally. To build a bimaterial system, we positioned this atomically resolved configuration next to the Si(001) substrate, initially leaving a gap of ∼12 Å between the two. The z-axis describes the direction perpendicular to the interface so formed, and the coordinate of the bottom surface of the PMB layer on this axis was determined as the average over the intrinsic surface roughness. Subsequently, the two slabs of material were brought closer to one another in steps of ∼0.2 Å. At this juncture, two procedures were followed. In one of them, the structures were not relaxed after repositioning, which serves to establish a noncontact adhesion baseline for comparison. The other procedure, resulting in wetting of the substrate, is based on prolonged relaxation after each such step. To this effect, the resulting configuration was briefly heated to 900 K (for 5 ps) to allow for accelerated relaxation while preventing structural disorder, and then quenched again to 300 K, where it was allowed to relax for at least another ∼100 ps. This procedure was repeated for each set of Lennard-Jones (LJ) potential parameters (σ_{Si}, ε_{Si}), used in this work to model the polyimide−Si interactions. In essence, the system has undergone a glass transition specific to each set of interface coupling parameters. Note that the transitions have taken place in a supported system, with one free surface and rigid constraints imposed in x- and y-directions. The ensuing implications will be discussed below. We stress that in the course of both quenching and room-temperature relaxation, periodic boundary conditions have been employed along the x- and y-directions of the simulation cell, but not in z-direction. The LJ parameters for Si (and, thus, for Si and PMB atoms, via the $\varepsilon_{Si-PI} = (\varepsilon_{Si}\varepsilon_{PI})^{1/2}$ relation) in the scheme, employed herein, were varied over a wide range. The optimal cutoff distance of the LJ potential was determined as $R_c \approx 16$ Å. The need for R_c optimization was based on ideas presented in refs 44 and 45. This value was fixed throughout all our simulations.

3. RESULTS AND DISCUSSION

3.1. Theoretical Foundation and Calculation Procedures. Despite a long history of inquiry, to date a satisfactory theoretical basis for the concepts of cohesion and adhesion has yet to be established.[46−48] In fact, the understanding of adhesion lags behind because of the increasing complexity of bi- and multimaterial systems emerging in response to the modern-era technological demands. The key quantity in analytical description of an adhesive interface is the work of adhesion or, alternatively, work of separation. The ideal work of separation is defined as

$$\tilde{W}_s = g_s + g_l - \gamma_i \quad (3)$$

where the g_s and g_l denote surface Gibbs free energies of substrate and deposited layer and γ_i is the free energy of the interface between the two, all normalized with respect to surface area. Equation 3 is known as the *Dupre* equation.[49] However, the Dupre equation is normally converted into the following form, which is more convenient for prevailing computational approaches:

$$W_s = E_s + E_l - E_{s+l} \quad (4)$$

In eq 4, W_s is the ideal work of separation, E_{s+l} is the total energy per unit interfacial area of the bimaterial system, including an interface, while E_s and E_l are the total energies per unit surface area of the system, where either adherent layer or the substrate has been replaced by vacuum. These quantities can be readily calculated from atomistic simulation data. Since both the interface and the free surfaces constitute similar deviations from the respective bulk structures, the cost of omitting entropic effects in eq 4 can be considered negligible, especially within a parametric study at room temperature.

Despite overwhelming interest and significant effort put toward developing descriptive frameworks for polymer layers deposited on covalent solid systems, the analytical treatments of the adhesion phenomenon are still in an early state. The most important insight, obtained insofar in this area, is the discovery of the so-called universal binding energy relation (UBER) by Smith and colleagues.[16−19] It was shown that a universal scaling relation of the separation energy with a characteristic length holds for bimetallic adhesion, metallic-to-covalent bonding in chemisorption, and a number of diatomic molecules.[19] Despite the apparent success of UBER, it has also been realized that the scaling relation breaks down for systems where dispersive vdW interactions are non-negligible.[17] This is

because UBER is based on the assumption that interface coupling is due to short-range overlap of atomic-like wave functions and ignores the contributions from long-range dispersive forces. Consequently, the description of various classes of bimaterials involving soft-matter and other polar materials, calls for a different theoretical framework. The analytical description of the adhesive behavior, governed by the vdW forces acting across an interface, is attributed to the pioneering works of de Boer[50] and Hamaker.[51] The approach, referred to as the de Boer−Hamaker (dBH) model, has been successful in predicting qualitative behaviors but lacks quantitative capabilities. The present work addresses some of the issues to consider in view of improving adhesion models.

3.2. Adhesion without Structural Relaxation. To obtain a reference state for pinpointing the effects of density, ordering, and the LJ potential well depth on the adhesion energy, we first investigated the behavior of an unrelaxed adherent layer. In this case, the constituents of the bimaterials system are not subject to structural relaxation, which would lead to a low-energy interface configuration. In other words, the structure of the reference state is kept independent of the choice of vdW parameters describing the interactions across the interface and, importantly, the PMB structure does not react to the presence of the substrate surface regardless of how close it is, that is, it does not wet this surface. Accordingly, we refer to the interfacial interactions associated with this type of configuration as noncontact adhesion. The homogeneous PMB layer was placed at a distance δz from the Si substrate top surface and the separation energy versus δz was computed for a set of potential well depths, ε_{Si}^{j} (j = 1−5). The results of simulations are shown in Figure 5. The magnitudes of ε_{Si}^{j} used are given in the figure caption. Five W_s versus δz curves are shown in Figure 5a. The corresponding interface forces were computed by taking numerical derivatives of the energy versus separation distance curves. In Figure 5b, the interface forces are plotted as a function of δz, for the same set of ε_{Si}^{j}. The behavior unveiled in this figure closely resembles that of UBER.[16−19] An increase in the coupling strength between substrate and PMB film naturally leads to an increase in the separation energy, at a rate proportional to the potential well depth, ε_{Si-PI}. The shape of all curves is similar to that of UBER, and the behavior can also be separated into three different regimes. The first regime, for separation distances below ∼0.5 Å, is characterized by a quadratic dependence of the separation energy on separation distance, revealing the harmonic stretching force acting between the PMB layer and substrate. This regime extends for no more than 1/4 of the average vdW range of the atoms in polyimide. The behavior changes to a sublinear increase at the inflection point, the result also predicted by UBER. This second regime extends to distances not exceeding the interaction potential radius. In the third regime, the energy asymptotically approaches a constant, approximately corresponding to the adhesion energy. The observed energy vs separation distance shape closely resembles those unveiled by the ab initio studies performed on metal and ceramic-metal systems.[16−19] The physical nature of the behavior is, of course, different. Indeed, in the case of crystalline structures adhesion is due to covalent bonds resulting from the overlap atomic orbital tails, while in our case the coupling forces are of dispersive (van der Waals) nature. However, certain features observed in the two bonding types may be similar, as, quantum mechanical calculations of the interactions between benzene rings have shown.[52] Accordingly, the self-consistent energy corresponds to the repulsive (R) part of the classical interaction potential, while the electron correlation energy accounts for the attractive (A) part of the potential.[52] Moreover, it was rigorously shown in the same paper that the correlation energy dependence on the separation distance closely follows $\sim -1/r^6$ behavior, which may account for the curve shape similarity.

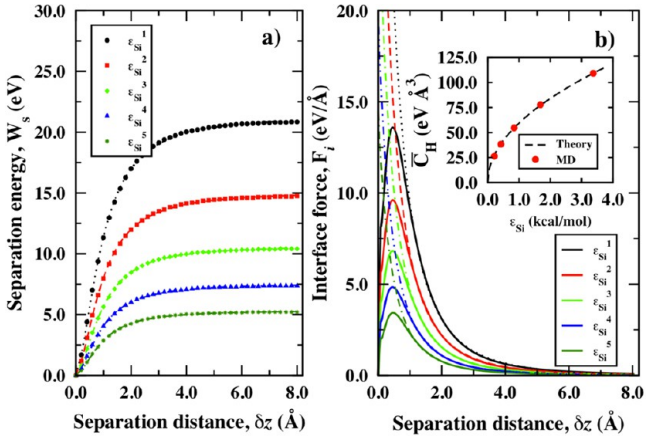

Figure 5. (a) Separation energy, W_s, versus separation distance, δz, is plotted for five magnitudes of the silicon potential well depths: (1) ε_{Si}^{1} = 3.27 kcal/mol, (2) ε_{Si}^{2} = 1.69 kcal/mol, (3) ε_{Si}^{3} = 0.84 kcal/mol, (4) ε_{Si}^{4} = 0.42 kcal/mol, and (5) ε_{Si}^{5} = 0.21 kcal/mol. (b) Interface force is shown as a function of separation distance for the same set of ε_{Si}^{j} (j = 1−5) magnitudes as in panel (a). Broken lines in panel b correspond to numerical fits of simulation data by eq 5. The inset in panel b shows the Hamaker constant dependence on ε_{Si}; the simulation data (solid circles) and theoretical fit (dashed line) are plotted.

The dependence of the interface force (and, thus, that of the stress) on the separation distance, shown in Figure 5b, is characteristic for the adhesion behaviors, as revealed by both atomistic and continuum studies.[53−57] While chemical bond effects superimpose onto dispersive contributions at a short distances, the long-range behavior is expected to be shaped predominantly by vdW forces. The experimentally observed range of vdW forces for Si−C is of the order of 1.6−2.0 nm,[45] that is, largely exceeding the influence of covalent bonding. It is at these large distances that we can qualitatively compare our observations with the existing analytical models of adhesion.[50,51] According to the dBH model, the force between two macroscopic bodies separated by a distance z_0 is

$$F_I = \frac{1}{6\pi}\left(\frac{C_6\pi^2\rho_{PI}\rho_{Si}}{z_0^3}\right) \quad (5)$$

where ρ_{PI} and ρ_{Si} are the densities of the two constituents of the bimaterial, and C_6 is the vdW coefficient in the $\sim -C_6/r^6$ dependence[51] [note that $C_6 \approx \varepsilon$]. To provide a direct comparison of simulation data with the de Boer−Hamaker model, eq 5 was fitted to simulation data for each interface coupling magnitude considered. As shown in Figure 5b, at relatively large separation distances the behavior is described well by eq 5, if C_6 is considered as a fitting constant (the only fitting constant in the procedure). This holds for all the values of LJ potential well depths considered here. Furthermore, we found that the ratio of the forces, for systems with varied ε, follow the relation: $F_1/F_2 \approx \varepsilon_1/\varepsilon_2$. Thus, the system under consideration obeys the dBH model[50,51] with a very high degree of accuracy. Discrepancies of ∼2−4% are the result of

inhomogeneity in the PMB layer density because of the discrete character of an atomistic representation and microporosity. The inset in Figure 5b shows the dependence of the Hamaker constant, $C_H = \pi^2 C \rho_{PI} \rho_{Si}$, on the potential well depth ε. The behavior is well described by the square-root law (note that $\varepsilon_{PI-Si} = (\varepsilon_{PI}\varepsilon_{Si})^{1/2}$), and thus, our results are in agreement with the predictions of the dBH model, valid for the description of dispersive interactions between solid bodies with homogeneous densities.

3.3. Adhesion Regimes. In contrast to the noncontact adhesion configurations described above, contact-adhesion is achieved when the PMB structure is allowed to adjust to the presence of the substrate. Hence, to create interfacial structures with varying adhesive energy, the computational procedure for generating fully relaxed polyimde−Si interfaces was repeated for a set of parameters ε_{Si}, ranging from 0.21 to 5.42 kcal/mol. The effective vdW radius of silicon was fixed at σ_{Si} = 1.24 Å throughout the simulations, which is close to the covalent radius. We have tested the simulation data for values of σ_{Si} varied in the range of 1.24−2.74 Å and found that qualitatively all our conclusions hold to a remarkable degree of agreement, and the quantitative results deviate only slightly. By varying ε_{Si} magnitudes in the aforementioned range, we observe a marked transition between two regimes in adhesive behavior at a critical value of interface coupling, ε^c_{Si}. The switchover between contact and noncontact adhesion is quantitatively evident from the work of adhesion, W_s, as a function of the potential well depth, ε_{Si}, as shown in Figure 6. In this figure, we compare W_s values

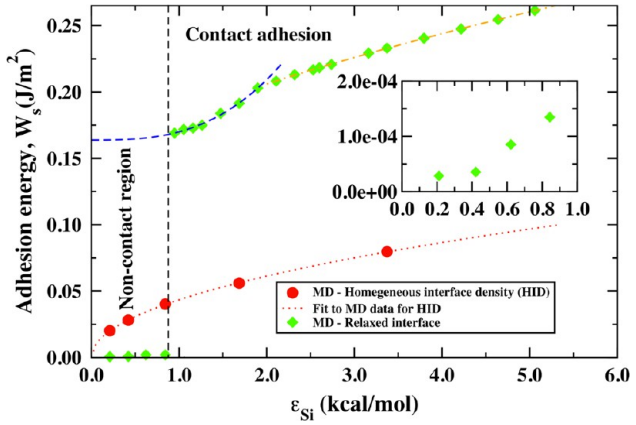

Figure 6. Separation energy, W_s, versus Lennard-Jones potential well depth, ε_{Si}, is shown for the cases of (i) homogeneous PMB layer on silicon (solid red circles) and (ii) fully relaxed, under condition of the Lennard-Jones coupling between polyimide and silicon, interfaces (solid green diamonds). The dotted line corresponds to best fit by the de Boer−Hamaker model, while the dashed and dash-dotted lines correspond to fits by scaling relationships (see text). The inset shows a magnified view of the data for the relaxed noncontact adhesion regime.

calculated for interfacial structures that are fully relaxed under the influence of the vdW coupling between silicon substrate and PMB layer to those of the nonrelaxed homogeneous PMB layer (reference states). For comparison, also shown in Figure 6a) is the prediction of the dBH model (dotted curve). In the noncontact regime, W_s is very weak and increases slowly with ε_{Si} (see inset of Figure 6). In this regime, the two parts of bimaterial system are coupled only through the long-range tails of dispersive forces, which can span a sizable gap, h_g ($\sigma_{Si} < h_g < R_c$), between them. The transition between the two regimes is characterized by an abrupt shift in W_s, followed by an accelerated increase of W_s that can be described by a power law

$$W_s \approx W_c + |\varepsilon_{Si} - \varepsilon^c_{Si}|^{\gamma} \quad (7)$$

where W_c is the adhesive energy at the transition $\varepsilon^c_{Si} \approx 0.92$ corresponds to the critical coupling, and the scaling exponent, γ = 2.86. Beyond $\varepsilon_{Si} \approx 2.0$ in the contact adhesion regime the adhesion energy continues to increase at a slower, slightly sublinear rate with ε_{Si}. This behavior can also be adequately described using a power law, with a scaling behavior of $W_s \approx \varepsilon_{Si}^{0.68}$. The comparison between the adhesive energies computed for relaxed and unrelaxed structures, the latter also being described by the dBH model,[50,51] shows that the continuum approach underestimates the adhesive energies for a given interaction strength. According to Figure 7, structural relaxation within the interfacial region accounts for a three- to four-fold increase in the work of adhesion. We furthermore expect that variation of the chemical nature of interfaces can be used to control the mechanical response of interfaces. However, a detailed investigation of this aspect is beyond the scope of this paper and will be deferred to future publications.

Molecular configurations associated with the contact and noncontact adhesion regimes are illustrated in Figure 7a and b. Both structures shown have been allowed to relax, and the difference between regimes depends on whether this relaxation leads to wetting of the substrate by PMB or detachment from it. To reconcile the notion of noncontact adhesion achieved following structural relaxation with the one obtained with nonrelaxed reference configurations, confirming the de Boer−Hamaker model, we examine structural developments for both regimes in detail. To this end, it is useful to elicit the concept of glass transition under confinement. While typically, the glass transition is associated with characteristic temperature dependent volumetric changes, the thermomechanical signatures of the glass transition are also apparent, when vitrification occurs in systems confined to a constant volume (isochoric glass transition). Similarly, a glass transition is observed as a function of the degree of cure for cross-linking polymers.[58,59]

Spatial confinement shifts the glass transition temperature, T_g, a well-known phenomenon that has been extensively researched.[60−64] With the present study we are able to isolate the effect of interfacial forces on the confinement of the glass-forming system. The noncontact adhesion interface structure shown in Figure 7a corresponds to vdW attraction strengths below the critical value ε^c_{Si}. Initially, that is, at temperatures above T_g, the PMB molecules closest to the substrate surface are at a distance corresponding approximately to the location of the interaction potential minimum. As the PMB layer is cooled it contracts because of the decrease in thermal motion. Meanwhile, the polyimide monomers are subject to two types of forces: a weak attraction to the substrate and comparatively stronger internal cohesive forces. As a result, at the free surface of the layer, the unbalanced forces exerted by the surface molecules exert a net attractive force on the PMB molecules inside the layer, which is directed away from the substrate and exceeds the interfacial bonding for as long as ε_{Si} is below critical magnitude. Hence, in this regime, as the PMB configuration vitrifies, it detaches from the substrate and recoils toward the center of the layer, resulting in the formation of a gap between the solid PMB and silicon surface. Essentially, the difference between nonrelaxed and relaxed noncontact adhesion is that for the former the gap between substrate and PMB layer is

dx.doi.org/10.1021/am3031163 | ACS Appl. Mater. Interfaces 2013, 5, 4702−4711

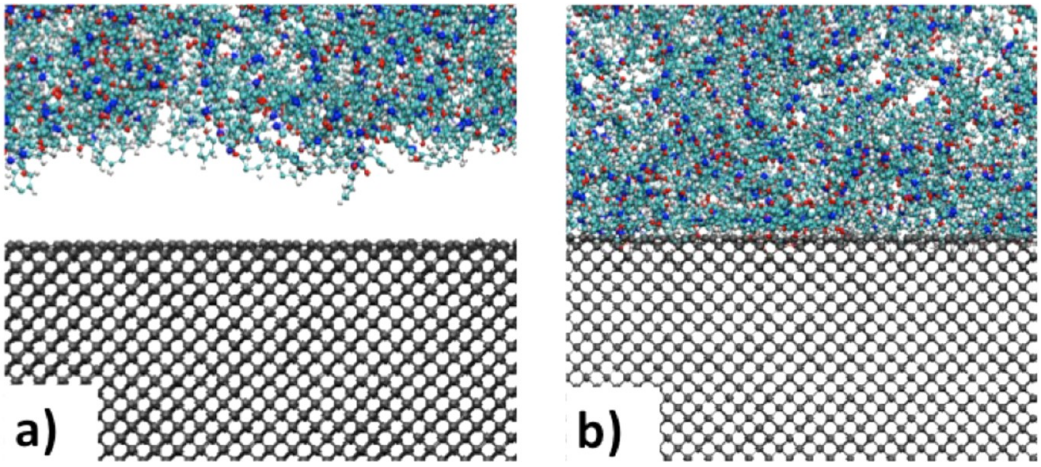

Figure 7. Snapshots of atomically resolved configurations of the interface regions are shown for the case of (a) noncontact adhesion interface (ε_{Si} = 0.211 kcal/mol and (b) the case of contact adhesion (ε_{Si} = 2.10 kcal/mol).

externally controlled while for the latter it results from internal cohesive forces.

In the noncontact regime, a small attraction still prevails across this gap due to the long-range effects of the vdW forces. Hence, even though the PMB layer shown in Figure 7a appears to have detached from the substrate, it remains physically tethered. In real materials, where substrate surfaces exhibit some degree of roughness, the contraction in the polymer layer is likely to occur in a less unidirectional manner than in the present study. As a result, near the crests of substrate surface mounds, the size of the gap will be smaller, and the overall force of adhesion will be stronger. However, because of the long-range nature of dispersive vdW interactions, substrate surface atoms at the bottom of crevices still exert attractive forces on the polyimide monomer layers resting on the crests. When ε_{Si} exceeds the critical value, ε^{c}_{Si}, as illustrated in Figure 7b, the balance of forces on the bulk of the PMB layer stemming from the substrate and the free surface is reversed. In this case, the PMB molecules adhere to the silicon surface, and, depending on the magnitude of the cross-interface attraction, the structure further reorganizes near the silicon surface and locally compacts as evident from with density profiles shown in Figure 8a and discussed in the next section. Moreover, when the attractive substrate forces become significant, voids form in the polyimide interior during vitrification (see Figure 8b). Indeed, under these circumstances there exists a simultaneous pull on the polyimide's interior toward the substrate due to the adhesive forces, and toward the free surface due to the polyimide surface tension (i.e., unbalanced interactions involving molecules at the free surface). In a sense, the appropriate balance between substrate adhesion and free surface tension can lead to conditions for isochoric glass transition.[60−62]

3.4. Interface Density Profiles. The balance of forces acting on the PMB layer discussed in the preceding section is reflected in the interfacial structures that develop. We first examine number density profiles, $n(z)$, across the layer. Two features stand out: densification immediately adjacent to the substrate and the formation of a region of dispersed paucity slightly below the free PMB surface. The atomic number density profiles of relaxed PMB structures near the interface with the silicon substrate for a representative selection of adhesion energies within the contact adhesion regime are shown in Figure 8a. Characteristic of all structures in this

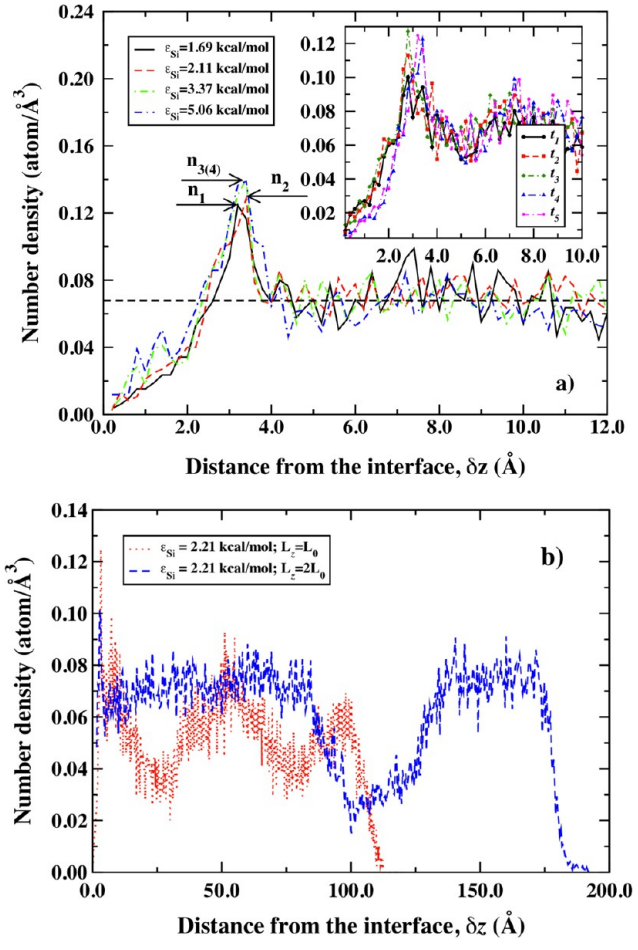

Figure 8. (a) Simulated number density profiles versus distance from the interface, δz, for bimaterial systems with the interface coupling, ε_{Si}, whose magnitudes are (1) 1.69, (2) 2.11, (3) 3.37, and (4) 5.06 kcal/mol. The horizontal dashed line shows the average density. Inset: Temporal evolution of the PMB layer density profiles for system with ε_{Si} = 2.11 kcal/mol and times: (1) $t_1 = 0.2 \times 10^6\ t_{MD}$, (2) $t_2 = 0.4 \times 10^6\ t_{MD}$, (3) $t_3 = 0.6 \times 10^6\ t_{MD}$, (4) $t_4 = 0.8 \times 10^6\ t_{MD}$, and (5) $t_5 = 1.0 \times 10^6\ t_{MD}$. (b) Simulated number density profiles versus distance from the interface, δz, are plotted for bimaterial systems with the interface coupling, ε_{Si} = 2.11 kcal/mol. Two differently sized systems are shown, one with twice the layer thickness of the other.

dx.doi.org/10.1021/am3031163 | ACS Appl. Mater. Interfaces 2013, 5, 4702−4711

regime, the profiles exhibit a well-pronounced peak at a distance corresponding roughly to 1.5 times the average Si−C equilibrium distance of the LJ potential (Figure 8a). The width of the peak increases with the coupling strength. Similarly, the height of the peak increases with ε_{Si} (from n_1 = 0.124 to n_2 = 0.128), but reaches a saturation height for coupling strength values exceeding ∼2.5 kcal/mol, at $n_{3(4)}$ = 0.139. This saturation has important implications for the adhesive behavior. The saturation of the peak height is accompanied by the appearance of distinct features in the density profile at less than 2 Å from the interface, which reflects the development of overconstrained configurations adjacent to the substrate, potentially causing structural instability. These configurations develop because the interface tension is so strong that molecular segments are no longer able to relax and are arrested in metastable states. The inset in Figure 8a shows the temporal evolution of the density profiles for systems with the interface coupling, ε_{Si} = 2.11 kcal/mol. This dynamics is characteristic for all systems that can undergo a significant degree of structural relaxation near the interface. Accordingly, the interface peak in the density profile develops gradually, starting with a broad low-magnitude feature that sharpens and grows into a distinct peak as structural relaxation progresses. In contrast to the configurations pinned to the substrate surface in case of large ε_{Si} values, considerable redistribution of material occurs at or near the interface. While the region below ∼2 Å appears to be depleted of polyimide units, the development of a density peak just above that distance is the result of the strong attraction of polyimide to the substrate surface, consistent with the nature of interface potential.

Finally, knowledge of the number density of atoms near the interface allows one to identify the structural origin of the adhesive energy by computing the energy density distribution according to

$$w_s(z) = \frac{\partial W_s}{\partial z} = \int_z^{z+dz} \frac{\partial E_{LJ}(z)}{\partial z} n(z)\, dz \tag{8}$$

where E_{LJ} is the Lennard-Jones potential energy acting between silicon atoms in the substrate and the atoms in the adjacent polyimide molecules. $w_S(z)$ is plotted as function of the distance from the substrate surface in Figure 9, and superimposed on this data is the atomic number density of the PMB film for reference. Accordingly, contributions to the adhesive energy sharply rise with decreasing distance from the interface at the upper flank of the density cusp, and remain relatively constant below this density maximum. Virtually all of the adhesive energy results from interactions between silicon and polyimide molecules at and below the density cusp. While attractive forces reach beyond the density cusp, it is at this location that polyimide molecules begin to experience the repulsion from silicon atoms in the top layers of the substrate. Hence, the density maximum is the result of the pressure exerted by polyimide molecules farther away from the interface onto polymer layers immediately adjacent to and repelled by the substrate surface. Interestingly, the unrelaxed configurations that develop at the interface under the influence of strong vdW attraction contribute significantly to the overall adhesive energy.

3.5. Structural Order at the Interface. Complementing the analysis of density profiles, we examined the interfacial structures for orientational ordering. To this end we define an order parameter (OP) tensor as

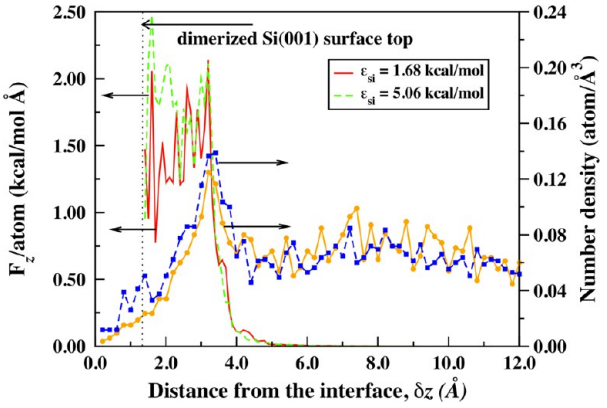

Figure 9. Normalized adhesive energy density per atom and number density as a function of the distance from the interface, δz. The origin of the z-axis is shifted down from the top silicon plane by ∼1.35 Å to account for polymer molecules penetrating the surface channels that form between dimer rows upon the silicon 2 × 1-reconstruction. Two different interface-coupling constants are considered, as listed in the figure legend.

$$Q_{\alpha\beta} = \left(\frac{3}{2}\langle e_{i\alpha} e_{i\beta}\rangle - \frac{1}{2} I_{\alpha\beta}\right) \tag{9}$$

where angular brackets denote both configuration and time averages, and I is the identity tensor. The unit vector for a molecule i, e_i, is taken along the molecule principal axis direction in the Cartesian coordinate system, the Greek indices being the Cartesian components of the orientation vector. The uniaxial order parameters can be computed by taking configuration and time averages over the second-rank Legendre polynomial, that is

$$\bar{Q}_{ua} = \frac{3}{2}\left\langle \cos(\theta_i)^2 - \frac{1}{2}\right\rangle \tag{10}$$

where θ_i is an angle between the molecule's longest axis and a reference direction of interest. For S_{zz} the reference direction points along the z-axis (perpendicular to the substrate surface), and for S_{xy} along the grooves of silicon surface formed due to the dimer-reconstruction. These two measures are shown in Figure 10 as a function of the distance from the interface (located at δz = 0). The dashed vertical line delineates the size of the gap that forms in the noncontact regime. While the data shows significant scatter, the following observations are unequivocal.

In the contact adhesion regime, the force of adhesion causes the rigid-rod molecular entities to align parallel to the interface (S_{zz} < 0.5) and along the dimer rows (S_{xy} > 0.5). This behavior occurs within a spatial range that appears to coincide with what would be vacated by polyimide structural units in the noncontact regime. Beyond this distance from the substrate surface, in the contact adhesion regime, molecular orientations seem to slightly favor orientations perpendicular to the interface ($S_{zz} \geq 0.5$), and increasingly random orientations relative to the dimer rows. (Note that S_{zy} = 0.5 would correspond to random orientations, if the polyimide molecules were placed in a plane; the third dimension available for molecule placement away from the interface provides many more orientations perpendicular to the trench axis than parallel to it that are random in space.) This behavior seems to become more accentuated upon approaching the free surface of the PMB layer. In comparison, weakening the interfacial bonding

dx.doi.org/10.1021/am3031163 | ACS Appl. Mater. Interfaces 2013, 5, 4702−4711

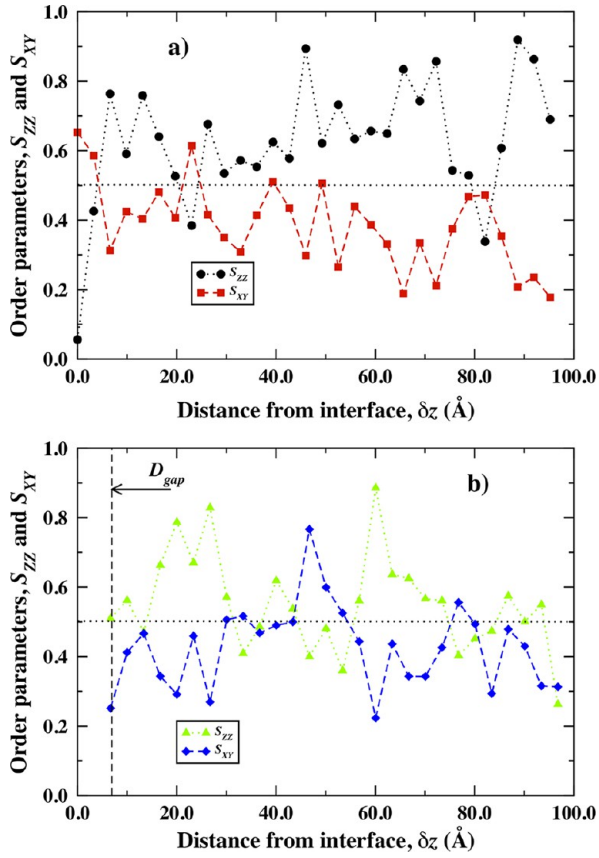

Figure 10. Order parameters, S_{zz} (orientation relative to the substrate surface normal) and S_{xy} (relative to the dimer row direction) as a function of the distance from the interface, δz. The two panes correspond to PMB on silicon systems with (a) ϵ_{Si} = 3.37 kcal/mol and (b) ϵ_{Si} = 0.84 kcal/mol. The dashed vertical line in the lower pane marks the gap arising at the interface for the weakly coupled system.

strength affects the OPs and orientational preferences somewhat. For one, S_{zz} no longer drops to a really low value near the substrate, and second, at larger distance from the interface both S_{zz} and S_{xy} assume values close to 0.5, which indicates more random orientations than in the contact-adhesion case, especially in the vicinity of the free surface.

We also examined the orientation of PMB molecules relative to each other. $\pi-\pi$ interactions between the aromatic rings of the PMB units tend to induce structural ordering in which these rings align parallel to each other, a phenomenon coined as $\pi-\pi$ stacking.[65] Short of accounting explicitly for the electronic structure of molecules, with the empirical potential we used these interactions must be reproduced with available nonbonding terms, such as vdW coupling. The degree of parallel stacking that can be achieved in this manner depends on the coupling strength and the distance from the substrate surface. We find that, in the contact adhesion regime, about two-thirds of PMB molecules arrange parallel to their nearest neighbors, as is expected for $\pi-\pi$ stacking, and that this ordering tendency decays rapidly as a function of the distance between molecules. Accordingly, clusters of parallel-stacked PMB units can be observed that span between six and eight layers. In close proximity to the interface, this stacking tendency is mildly enhanced, but by no more than 4% for the strongest interfacial coupling strength.

4. CONCLUSION

We performed a comprehensive atomistic simulation study of adhesion of aromatic poly-[(4,4′-diphenylene) pyromellitimide] adherent layers onto a dimer-reconstructed Si(001) substrate surface. The adhesive energy (or work of adhesion), that is, the difference between the energy of adherent and substrate in contact with each other and that of the two slabs separated by a distance that prevents any interactions between them, was computed for two scenarios. In one of them, the silicon and PMB molecular slabs were positions in close proximity of each other without allowing either structure to undergo structural relaxation in response to the trans-interfacial forces. This prevents wetting of the substrate by the polymer, that is, molecular rearrangements in the polymer to conform to the substrate surface structure, and leads to a noncontact adhesion regime. This regime is characterized by relatively weak adhesive forces that, for a range of interaction parameters typically associated with physisorption, can be perfectly described by the de Boer−Hamaker model, which had been developed based on a continuum description of matter.

In the other scenario, PMB layers undergo substantial structural reorganization in response to the attractive forces from the substrate. Under these conditions we observe a transition between noncontact and contact adhesion upon exceeding a critical value of the interaction strength between polymer and substrate. The wetting layer that develops in the contact adhesion regime exhibits a density cusp at around 3.2 Å from the interface, as a direct consequence of the attraction of polyimide units toward the substrate. The cusp intensity increases with the van der Waals interaction strength, but saturates when the attractive forces balance the repulsion between polymer molecules. The stronger the attraction to the substrate the more the rigid monomer units of the polymer align parallel to the substrate surface, albeit, while statistically significant, this ordering is not visually evident. Most importantly, structural relaxation near the interface results in a three- to three-fold increase in the adhesive energy compared to nonrelaxed configurations, demonstrating the importance of accurately describing structural details of interfaces at the atomic level in order to achieve reliable predictions of interfacial strengths. The present study does not take the role of oxide or nitride passivation layers into account, which is known to lead to further enhancement of interfacial strength, nor do we consider aspects of dynamic loading, which underlie experimentally determined interfacial fracture strengths.

AUTHOR INFORMATION

Corresponding Author

*E-mail: kieffer@umich.edu.

Notes

The authors declare no competing financial interest.

ACKNOWLEDGMENTS

This research was supported by the National Science Foundation, through Industrial Research Initiative (Grant No. NSF IRI-10-07322). The computational facilities of the CAC at the University of Michigan were used to perform all the simulations, reported herein.

REFERENCES

(1) Lupinski, J. G., Moore, R. S., Eds. Polymeric materials for electronic packaging and interconnection. In *Polymeric Materials for*

Electronic Packaging and Interconnection; ACS Symposium Series, Vol. *407*; American Chemical Society: Washington, DC, 1989.
(2) Tummala, R. R.; Keyer, R. W.; Grobman, W. D.; Kapen, S. In *Microelectronics Packaging Handbook*; Tummala, R. R.; Rymaszewski, E. J., Eds.; Van Nostrand Reinhold: New York, 1989.
(3) Sroog, C. E. *J. Polym. Sci., Part D: Macromol. Rev.* **1976**, *11*, 161−208. Wilson, D. *Polyimides*; Chapman & Hall: London, 1990.
(4) Wilson, A. M. In *Polyimides: Synthesis, Characterization, and Applications*; Mittal, K. L., Ed.; Plenum: New York, 1984.
(5) Pocius, A. V. *Adhesion and Adhesive Technologies*, 2nd ed.; Hanser Publications: University Heights, IL, 2002.
(6) Mui, C.; Wang, G. T.; Bent, S. F.; Musgrave, C. B. *J. Chem. Phys.* **2001**, *114*, 10170−10180.
(7) Wang, B.; Zheng, X. L.; Michl, J.; Foley, E. T.; Hersam, M. C.; Bilic, A.; Crossley, A. M.; Reimers, J. R.; Hush, N. S. *Nanotechnology* **2004**, *15*, 324−332.
(8) Zhu, Z. M.; Srivastava, A.; Osgood, R. M., Jr. *J. Phys. Chem. B* **2003**, *107*, 13939−13948.
(9) Loscutoff, P. W.; Wong, K. T.; Bent, S. F. *Surf. Sci.* **2010**, *604*, 1791−1799.
(10) Hoh, H. Y.; Ouyang, T.; Sullivan, M. B.; Wu, P.; Nesladek, M.; Loh, K. P. *Langmuir* **2010**, *26*, 3286−3291.
(11) Simo, J. C.; Ju, J. W. *Int. J. Solids Struct.* **1987**, *23*, 821−840.
(12) Simo, J. C.; Ju, J. W. *Int. J. Solids Struct.* **1987**, *23*, 841−869.
(13) Nicholson, D. W. *J. Adhes.* **1979**, *10*, 255−260.
(14) Matous, K.; Kulkarni, M. G.; Geubelle, P. H. *J. Mech. Phys. Solids* **2008**, *56*, 1511−1533.
(15) Kulkarni, M. G.; Geubelle, P. H.; Matous, K. *Mech. Mater.* **2009**, *41*, 573−583.
(16) Rose, J. H.; Ferrante, J.; Smith, J. R. *Phys. Rev. Lett.* **1981**, *47*, 675−678.
(17) Rose, J. H.; Smith, J. R.; Ferrante, J. *Phys. Rev. B* **1983**, *28*, 1835−1845.
(18) Banerjea, A.; Smith, J. R. *Phys. Rev. B* **1988**, *37*, 6632−6645.
(19) Smith, J. R.; Hong, T.; Srolovitz, D. J. *Phys. Rev. Lett.* **1994**, *72*, 4021−4024.
(20) Baljon, A. R. C.; Robbins, M. O. *Science* **1996**, *271*, 482−484.
(21) Gersappe, D.; Robbins, M. O. *Europhys. Lett.* **1999**, *48*, 150−155.
(22) Henry, D. J.; Yiapanis, G.; Evans, E.; Yarovsky, I. *J. Phys. Chem.* **2005**, *109*, 17224−17231.
(23) Weaver, C. *Adhesion: Fundamentals and Practice*; U.K. Ministry of Technology, Maclaren: London, 1969; pp 46−57.
(24) Sidorovich, A. V.; Baklagina, Y. G.; Kenarov, A. V.; Nadezhdin, Yu. S.; Adrova, N. A.; Florinsky, F. S. *J. Polym. Sci., Polym. Symp.* **1977**, *58*, 359−367.
(25) Obata, Y.; Okuyama, K.; Kurihara, S.; Kitano, Y.; Jinda, T. *Macromolecules* **1995**, *28*, 1547−1551.
(26) Allen, M. P.; Tildesley, D. J. *Computer Simulation of Liquids*; Clarendon Press: Oxford, U.K., 1989.
(27) Smith, W.; Forester, T. R. *J. Mol. Graph.* **1996**, *14*, 136−141.
(28) Smith, W.; Yong, C. W.; Rodger, P. M. *Mol. Simul.* **2002**, *28*, 385−471.
(29) Smith, W. *Mol. Simul.* **2006**, *32*, 933−933.
(30) Cornell, W. D.; Cieplak, P.; Bayly, C. I.; Gould, I. R.; Merz, K. M., Jr.; Ferguson, D. M.; Spellmeyer, D. C.; Fox, T.; Caldwell, J. W.; Kollman, P. A. *J. Am. Chem. Soc.* **1995**, *117*, 5179−5197.
(31) Ewald, P. P. *Ann. Phys.* **1921**, *64*, 253−287.
(32) Stendardo, E.; Pedone, A.; Cimino, P.; Menziani, M. C.; Crescenzi, O.; Barone, V. *Phys. Chem. Chem. Phys.* **2010**, *12*, 11697−11709.
(33) Frisch, M. J.; Trucks, G. W.; Schlegel, H. B.; Scuseria, G. E.; Robb, M. A.; Cheeseman, J. R.; Scalmani, G.; Barone, V.; Mennucci, B.; Petersson, G. A.; Nakatsuji, H.; Caricato, M.; Li, X.; Hratchian, H. P.; Izmaylov, A. F.; Bloino, J.; Zheng, G.; Sonnenberg, J. L.; Hada, M.; Ehara, M.; Toyota, K.; Fukuda, R.; Hasegawa, J.; Ishida, M.; Nakajima, T.; Honda, Y.; Kitao, O.; Nakai, H.; Vreven, T.; Montgomery, J. A., Jr.; Peralta, J. E.; Ogliaro, F.; Bearpark, M.; Heyd, J. J.; Brothers, E.; Kudin, K. N.; Staroverov, V. N.; Kobayashi, R.; Normand, J.; Raghavachari, K.; Rendell, A.; Burant, J. C.; Iyengar, S. S.; Tomasi, J.; Cossi, M.; Rega, N.; Millam, J. M.; Klene, M.; Knox, J. E.; Cross, J. B.; Bakken, V.; Adamo, C.; Jaramillo, J.; Gomperts, R.; Stratmann, R. E.; Yazyev, O.; Austin, A. J.; Cammi, R.; Pomelli, C.; Ochterski, J. W.; Martin, R. L.; Morokuma, K.; Zakrzewski, V. G.; Voth, G. A.; Salvador, P.; Dannenberg, J. J.; Dapprich, S.; Daniels, A. D.; Farkas, O.; Foresman, J. B.; Ortiz, J. V.; Cioslowski, J.; Fox, D. J. *Gaussian 09*, revision A.02; Gaussian, Inc.: Wallingford, CT, 2009.
(34) Besler, B. H.; Merz, K. M., Jr.; Kollman, P. A. *J. Comput. Chem.* **1990**, *11*, 431−439.
(35) Singh, U. C.; Kollman, P. A. *J. Comput. Chem.* **1984**, *5*, 129−145.
(36) Theodorou, D. N.; Suter, U. W. *Macromolecules* **1985**, *18*, 1467−1478.
(37) Berendsen, H. J. C.; Postma, J. P. M.; Van Gunsteren, W. F.; Di Nola, A.; Haak, J. R. J. *Chem. Phys.* **1984**, *81*, 3684−3690.
(38) van de Waal, B. W. *J. Non-Cryst. Solids* **1995**, *189*, 118−128.
(39) Roe, R. J. *Adv. Pol. Sci.* **1994**, *116*, 111−144.
(40) Sazanov, Y. N.; Szekely, T.; Gribanov, A. V.; Bertoti, I.; Antonova, T. A.; Toth, A. *Acta Polimerica* **1988**, *39*, 516−523.
(41) Numata, S.; Miwa, T. *Polymer* **1989**, *30*, 1170−1174.
(42) Tersoff, J. *Phys. Rev. B* **1988**, *38*, 9902−9905.
(43) Unni, K. N. N.; Dabos-Seignon, S.; Pandey, A. K.; Nunzi, J.-M. *Solid-State Electron.* **2008**, *52*, 179−181.
(44) Ruvinsky, A. M.; Vakser, I. A. *Bioinformatics* **2009**, *25*, 1132−1136.
(45) Bruch, L. W. *Phys. Rev. B* **2005**, *72*, 033410.
(46) Lennard-Jones, J. E. *Proc. Phys. Soc.* **1931**, *43*, 461−482.
(47) Israelachvili, J. N. *Intermolecular and Surface Forces*; Academic Press: New York, 1985.
(48) Politi, R. E. In *High Temperature Polymer Matrix Composites*; Serafini, T. T., Ed.; Noyes Data Corp.: Park Ridge, NJ, 1987.
(49) de Gennes, P. G. *Rev. Mod. Phys.* **1985**, *57*, 827−863.
(50) de Boer, J. H. *Trans. Faraday Soc.* **1936**, *32*, 10−37.
(51) Hamaker, H. C. *Physica* **1937**, *4*, 1058−1072.
(52) Jaffe, R. L.; Smith, G. D. *J. Chem. Phys.* **1996**, *105*, 2780−2788.
(53) Finnis, M. W. *J. Phys: Cond. Mat.* **1996**, *8*, 5811−5836.
(54) Needleman, A. *J. Appl. Mech.* **1987**, *54*, 525−531.
(55) Needleman, A.; Nutt, S. A. *Adv. Fract. Res.* **1989**, *3*, 2211−2218.
(56) Needleman, A. *Int. J. Fract.* **1990**, *42*, 21−40.
(57) Hayes, R. L.; Ortiz, M.; Carter, E. A. *Phys. Rev. B* **2004**, *69*, 172104.
(58) Müller, U.; Philipp, M.; Gervais, P. C.; Possart, W.; Wehlack, C.; Kieffer, J.; Sanctuary, R.; Krüger, J. K. *New J. Phys.* **2010**, *12*, 083036.
(59) Colucci, D. M.; McKenna, G. B.; Filliben, J. J.; Lee, A.; Curliss, D. B.; Bowman, K. B.; Russell, J. D. *J. Polym. Sci., Part B* **1997**, *35*, 1561−1573.
(60) Yang, L.; Srolovitz, D. J.; Yee, A. F. *J. Chem. Phys.* **1999**, *110*, 7058−7069.
(61) Consolati, G.; Levi, M.; Messa, L.; Tieghi, G. *Europhys. Lett.* **2001**, *53*, 497−503.
(62) Kim, C.; Facchetti, A.; Marks, T. J. *J. Am. Chem. Soc.* **2009**, *131*, 9122−9132.
(63) Paeng, K.; Swallen, S. F.; Ediger, M. D. *J. Am. Chem. Soc.* **2011**, *133*, 8444−8447.
(64) Wake, W. C. *Polymer* **1978**, *19*, 291−308.
(65) Hunter, C. A.; Sanders, J. K. M. *J. Am. Chem. Soc.* **1990**, *112*, 5525−5534.